Deepening of radiation belt over South Atlantic Anomaly region

Pankaj K. Soni[1]*, Bharati Kakad[1], and Amar Kakad[1]

[1]Indian Institute of Geomagnetism, New Panvel, Navi Mumbai, India 410218.

Key Points:

- Weakening of Earths magnetic field in the SAA region is pushing radiation belt particles towards the Earth at the rate of 4.1±0.1 kms/year.
- During 1900-2020 the radiation belt particles have been pushed 480 kms closer to the Earth in SAA region.
- The deeper penetration of the energetic particles will pose greater risks to our satellites, life and climate.

*Indian Institute of Geomagnetism, New Panvel, Navi Mumbai, India 410218.

Corresponding author: Pankaj K. Soni, pankajkumar.s@iigm.res.in, pankajs123321@gmail.com

Abstract

The geomagnetic field has an unusual weak spot over South America and the South Atlantic Ocean, called South Atlantic Anomaly (SAA). The magnetospheric particles trapped in this field penetrate deep into the atmosphere over the SAA resulting in lower inner boundary of the radiation belt. Over the past 400 years, the magnetic field in the SAA region has decreased consistently. This study shows that the weakened geomagnetic field has a bearing on the position of the inner boundary of the radiation belt. The present simulation revealed that the inner boundary of the radiation belt over the SAA region is moving earthward at the rate of 4.1±0.1 km/year and that earthward penetration of energetic particles has increased by ≈480 km during period 1900-2020. If the geomagnetic field in the SAA region continues to decrease, the resulting deepening of the radiation belt will pose increased risks to our satellites, life, and climate.

Plain Language Summary

The geomagnetic field protects us from highly energetic particles originated from Sun. However, a region like SAA, where the geomagnetic field is weak compared to other parts of the globe, is the favorite gateway for them to reach closer to the Earth. Over this region, the radiation belt possesses a deeper boundary in the Earths upper atmosphere. The observations have shown that the geomagnetic field in the SAA region has decreased significantly in the last few decades. The effect of such a declining magnetic field on the lower boundary of the radiation belt over SAA is crucial and not examined so far. We have performed simulations to quantify the effect of this weakened magnetic field on the penetration altitudes of the energetic radiation belt particles. Our study demonstrates that the weakening of the geomagnetic field in the SAA region pushing the radiation belt particles towards the Earth at the rate of 4.1kms/year. The most important finding is that the radiation belt particles have been pushed ≈480km closer to the Earth in SAA region during 1900-2020. This finding suggests that the deeper penetration of the radiation belt particles will pose greater risks to our satellites, life, and climate in future.

1 Introduction

The Earth possesses a magnetic field that forms a magnetic field cavity, termed magnetosphere, around the planet. The magnetic field deflects highly energetic charged solar wind particles approaching the Earth, thereby acting as a protective shield for life on Earth. Some of the charged particles are trapped in the Earth's magnetic field, and they populate different regions of the magnetosphere such as the magnetosheath and plasmasphere, apart from the ring current and radiation belts (Ebihara & Miyoshi, 2011). The radiation belts are regions where energetic charged particles are held by the geomagnetic field (Millan & Baker, 2012). The Earth's magnetosphere includes the inner and outer radiation belts, and the energetic charged particles therein have adverse effect on spacecraft and satellites. The inner belt is located in the region between one and three Earth radii (Earths radius = 6371 km) and contains protons and electrons with energies of the order of hundreds of MeV and keV, respectively (Ripoll et al., 2020).

The trapped particles perform three quasi-periodic motions: gyration, bounce, and drift. A set of three adiabatic invariants defines their stable drift shells in which they encircle the Earth (Mukherjee & Rajaram, 1981; Northrop & Teller, 1960). These bouncing-drifting magnetospheric charged particles approach closer to the Earth in the South Atlantic Anomaly (SAA) region, where the magnetic field is weaker compared with other parts of the globe. The SAA is widely referred to as a dent in the Earth's magnetic field and similar to the polar regions, where magnetic field lines are open, it is a favorite gateway for the energetic particles of the magnetosphere (Heirtzler, 2002). The inner radiation belt is closest to the Earth over the SAA region, posing potentially high risks to

our satellites, life, and climate because of the extreme radiation levels in the region (Rodrigues, Taschetto, Gupta, & Foltz, 2019; Zhu & Liu, 2020). Over the past 400 years, the magnetic field in the SAA region has decreased consistently(Gillet, Jault, Finlay, & Olsen, 2013). The effect of the weakening of the magnetic field in the SAA region on the lower boundary of the inner radiation belt has not been investigated so far. A question that arises is, if the geomagnetic field continues to decrease at the present rate, then how much closer will energetic charged particles come in the SAA region? The present study addressed this question.

We performed a three-dimensional test-particle simulation of energetic charged particles trapped in Earth's magnetosphere by the geomagnetic field, which was realistically modeled by utilizing coefficients of the latest (13th generation) International Geomagnetic Reference Field (IGRF) model (Alken et al., 09 Sep, 2020). The penetration level of the inner radiation belts charged particles in the SAA region during the period 1900-2020 is quantified by considering the secular variation in the geomagnetic field. The IGRF is a well-established, widely used model (Thébault et al., 2015) that can be used to understand the secular variation of the Earth's intrinsic magnetic field, which is generated by the geodynamo (Liu & Olson, 2009; Suttie, Holme, Hill, & Shaw, 2011). Quantitative estimates of the penetration altitude of the radiation belts energetic charged particles in the SAA region can help to understand the possible risks to low orbiting satellites, life, and climate in the near future.

2 Methodology

2.1 Model Structure

We traced the motion of a relativistic charged particle with charge q and mass m in the presence of the Earth's magnetic field by considering the following governing equations Öztürk (2012); Soni, Kakad, and Kakad (2020a, 2020b):

$$\frac{d\boldsymbol{R}}{dt} = \frac{\gamma m v^2}{2qB^2}\left(1 + \frac{v_\parallel^2}{v^2}\right)\hat{\boldsymbol{b}} \times \nabla B + v_\parallel \hat{\boldsymbol{b}}, \tag{1}$$

$$\frac{dv_\parallel}{dt} = -\frac{\mu}{\gamma^2 m}\hat{\boldsymbol{b}}.\nabla B. \tag{2}$$

Here, $\boldsymbol{R}$ is the position of the guiding center, γ is the relativistic factor given by $\gamma = (1 - v^2/c^2)^{-1/2}$, μ is the magnetic moment given by $\mu = \gamma^2 m v_\perp^2/2B$, $v_\parallel$, and $v_\perp$ are the parallel and perpendicular components of the velocity vector, and $\hat{b}$ is the unit vector in the direction of the local magnetic field. Equations (1) and (2) pertain to the guiding-center- approximation, wherein the motion of a charged particle is averaged over a gyration to trace its guiding center. These equations were solved numerically by using a sixth-order Runge-Kutta method. The input parameters in the simulation were charge q, mass m, kinetic energy E_k, pitch angle α, and initial position $[x_0 = rsin\theta cos(\phi)$, $y_0 = rsin\theta sin\phi$, $z_0 = rcos\theta]$. Here, r, θ, and ϕ are the geocentric distance, co-latitude, and longitude, respectively. The geographic latitude λ is given by $\lambda = 90^\circ - \theta$. The geographic longitude ϕ was measured positive eastward from Greenwich, and it ranged from 0° to 360°. The initial velocity v_0 of a particle was estimated from its energy as follows:

$$v = c\sqrt{1 - (\frac{m_0 c^2}{m_0 c^2 + E_k})^2}. \tag{3}$$

Particles with energy E_k can enter the Earth's magnetosphere from any longitude. The angle between a particle's velocity vector $\vec{v}$ and the local magnetic field $\vec{B}$ is termed pitch angle. We placed a particle in space at the initial position $[r, \theta, \phi]$ with the velocity components $v_\parallel = v_0 cos(\alpha_{eq})$ and $v_\perp = \sqrt{v_x^2 + v_y^2}$. Here, $v_x = v_0 cos\alpha_{eq} cos\psi$, $v_y = v_0 sin\alpha_{eq} sin\psi$, α_{eq} is the equatorial pitch angle of the particle, and $\psi = \phi + 180^\circ$ is the gyro-phase of

the particle. The gyro-phase is the angle made by the perpendicular velocity component with the positive x-direction and it decides the particle's position in the horizontal xy-plane. The test-particle simulations were performed in the Cartesian coordinate system, with the positive x, y, and z directions being the upward, eastward, and northward directions. The output of the simulation was converted into the spherical coordinate system $[r, \theta, \phi]$.

2.2 Magnetic Field Configuration

It was important to use a realistic model of the Earth's magnetic field in the simulation. Mathematically, the Earth's magnetic field $\boldsymbol{B}$ can be described as the negative gradient of a scalar potential function V:

$$\boldsymbol{B} = -\nabla V. \tag{4}$$

V can be represented by a series of spherical harmonics:

$$V(r,\theta,\phi) = R_e \sum_{n=1}^{N} \left(\frac{R_e}{r}\right)^{n+1} \sum_{m=0}^{n} [g_n^m cos(m\phi) + h_n^m sin(m\phi)] P_n^m(\theta). \tag{5}$$

The set of Gaussian coefficients g_n^m and h_n^m were obtained from the latest 13th generation International Geomagnetic Reference Field model `https://www.ngdc.noaa.gov/IAGA/vmod/igrf.html`. A working group constituted by the International Association of Geomagnetism and Aeronomy examines high-quality and globally distributed observations of the geomagnetic field and updates the coefficients every five years. $P_n^m(\theta)$ represents the Schmidt quasi-normalized associated Legendre functions of degree n and order m. We implemented these mathematical steps in the computation by following Navabi et al.Navabi and Barati (2017). The scalar potential defined in Eq. (5) was used together with Eq. (4) to obtain the magnetic field components $[B_r, B_\theta, B_\phi]$, which can be converted into Cartesian coordinates $[B_x, B_y, B_z]$. These magnetic field components were then used in Eqs. (1), and (2) to simulate particle motion.

3 Results

The Earth's magnetic field can be analytically represented by a series of spherical harmonics that include Gaussian coefficients and associated Legendre polynomials (Navabi & Barati, 2017). These spherical harmonic coefficients can be derived from long-term data obtained from ground magnetic observatories and magnetometers onboard low Earth-orbiting satellites. The IGRF is a mathematical model widely used to determine the Earths magnetic field at a location, mainly the large-scale internal contribution (Alken et al., 09 Sep, 2020). We used the most recent IGRF models (IGRF-13) coefficients to compute the Earth's magnetic field as a function of latitude, longitude, and altitude during 1900-2020. Figures 1(a) and 1(b) show maps of the total intensity of the surface geomagnetic field for the years 1900 and 2020, respectively. The most prominent anomalous feature is the low magnetic field over the South Atlantic region, shown in blue. Figure 1 indicates that the magnetic field in the SAA region decreased from 1900 to 2020 and that the area of the region increased significantly. The consistent decrease in the Earth's magnetic field in the SAA region has been actively studied by researchers (S. A. Campuzano, Gómez-Paccard, Pavón-Carrasco, & Osete, 2019; Finlay, Olsen, Kotsiaros, Gillet, & Tøffner-Clausen, 2016).

Energetic charged particles entering the Earth's magnetosphere penetrate to a lower altitude in the SAA region because of the weaker magnetic field in the region. We carried out a three-dimensional test-particle simulation to analyze the effect of spatiotemporal variations in the geomagnetic field on the minimum penetration altitude $H_{\min}$ of the inner radiation belt particles. In the simulation model, we solved the Newton-Lorentz equation by considering a geomagnetic field that was modeled using IGRF-13. We obtained Gaussian coefficients for the period 1900 to 2020 at 10-year intervals and tracked

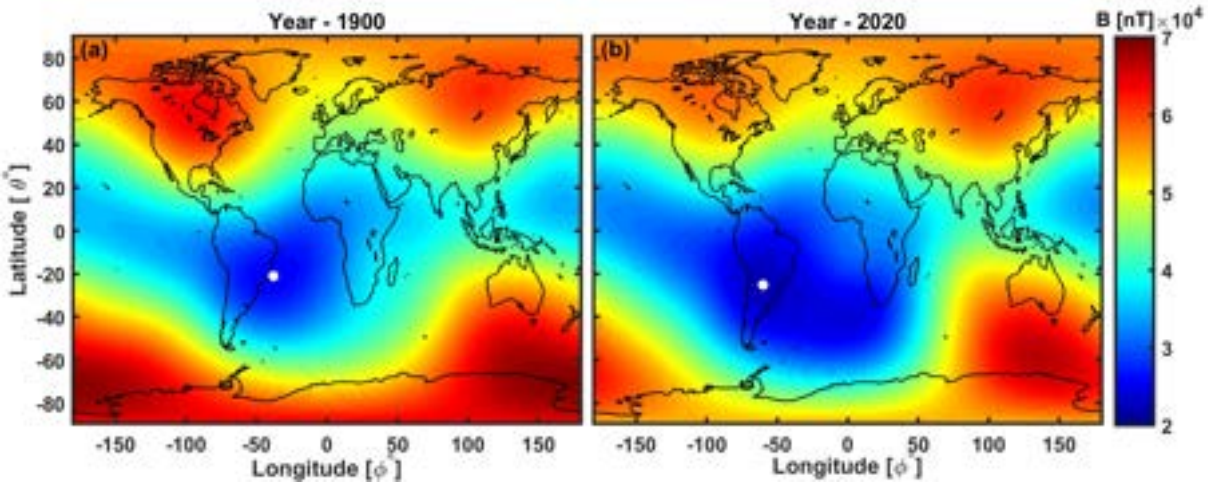

Figure 1. Variation of the Earth's surface magnetic field for the years (a) 1900 and (b) 2020 estimated from the IGRF-13 model. The white dots represent surface locations with the lowest magnetic field strength in the SAA region.

the trajectory of 10 MeV protons initially located at L =2 and L =3. The L-value gives the distance of a magnetic field line from the center of the Earth at the magnetic equator in units of Earth radii R_e, with R_e =6371kms. Thus, L =2 and 3 respectively corresponds to an initial altitude (H_0) of $1R_e$ and $2R_e$ above the surface of the Earth in the equatorial plane at initial time t=0. The proton was introduced at the geocentric equator outside the anomaly region with an equatorial pitch angle α_{eq} of 89° and the simulation was carried out for one azimuth drift around the Earth. The pitch angle is the angle between the magnetic field vector and the particle's velocity vector. Protons entering the Earth's equatorial region have large pitch angles, with a peak close to 90°, in their distribution (M. W. Chen et al., 1999). Therefore, we chose a large value for the pitch angle.

The simulated trajectory of the 10 MeV proton initially located at L =2 in the geocentric equatorial plane and at the longitude $\phi_0 = 120°$ is shown in Figure 2 for the year 2020. The trajectory was obtained under the guiding-center approximation, implying that the gyro-motion of the proton around the magnetic field line was averaged over a gyration to trace the guiding center of the particle. Figure 2(a) clearly shows the proton bouncing along magnetic field lines and drifting around the Earth. The color bar represents the magnetic field strength at the surface of the Earth, and the anomaly region corresponds to blue color. The tilt of the magnetic axis with respect to the geographic axis of the Earth along with the low magnetic field in the SAA region result in the asymmetry in the proton motion across the equatorial plane. As the bouncing-drifting proton approaches the SAA region, it penetrates the Earths atmosphere to reach lower altitudes. This earthward movement of the proton occurs because the proton encounters gradients in the magnetic field during its azimuthal drift across the SAA region. This gradient-B driftF. F. Chen et al. (1984) results in the guiding center of the proton experiencing a force in the $\vec{B}\times\nabla B$ direction. The two-dimensional trajectory of the proton as seen from over the south geomagnetic pole is shown in Figure 2(b), where the Earth is represented by a sphere centered at the origin. The color bar represents the radial distance r of the proton from the center of the Earth, in units of Earth radii. The trajectory shown in Figure 2 reveals that a bounce-drifting proton introducd at L =2 approaches closer to the Earth in the longitudinal zone 130°W to 20°E, which corresponds to the SAA region. This longitudinal zone is marked by an arrow in Figure 2(b).

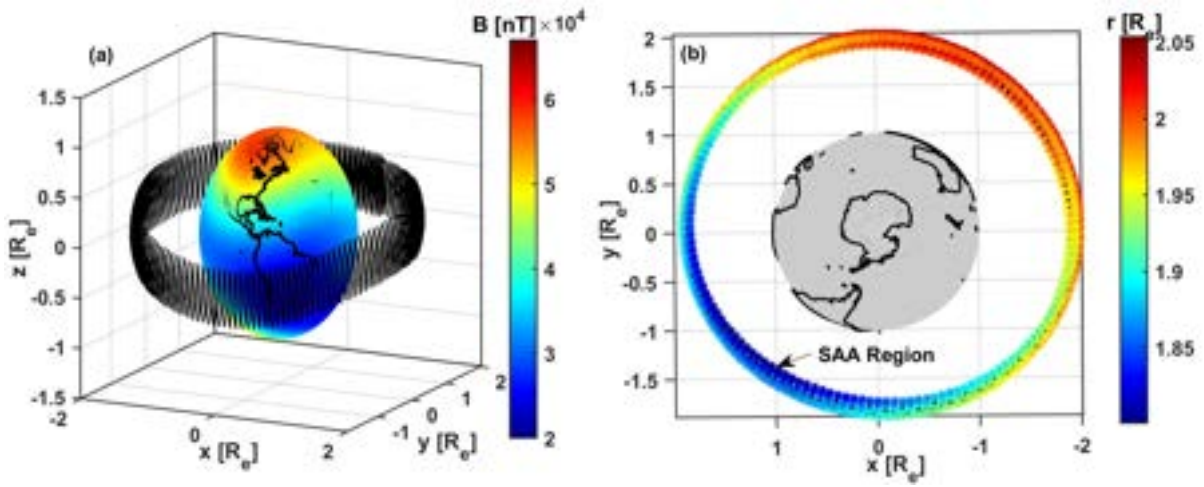

Figure 2. The trajectory of a 10 MeV proton with a pitch angle of 89° at L = 2 in the Earth's magnetic field for 150 s. (a) The color bar represents the magnetic field intensity, and the proton trajectory is shown by the black ring. (b) A top view of the protons motion as seen from the south geomagnetic pole. The color bar represents the protons radial distance, r from the Earths center.

We converted the position of the proton from Cartesian [x, y, z] to spherical [r, θ, ϕ] coordinates at each time step. Here θ and ϕ represent the geographic latitude and longitude of the proton at a given time, respectively. The protons altitude from the Earths surface was estimated as $H = r - R_e$ during its complete drift around the Earth. The variation of the protons altitude as a function of the longitude is shown in Figure 3 for the years 2020 (red) and 1900 (blue). Figures 3(a) and 3(b) show the variation for the protons initially placed at L =2 and L =3, respectively. The variation of the altitude clearly shows an inverted-bell shape, with the lowest altitude being in the SAA region owing to the lower magnetic field strength of the region. Although the equatorial pitch angle was very large ($\alpha_{eq} = 89°$), the asymmetry of the magnetic field significantly affected the protons bounce motion. Thus, the spread in the altitude of the proton at a fixed longitude for both years (depicted by red and blue dots) is attributed to the bounce motion of the proton. We averaged the altitude $\overline{H}$ over the longitudinal range of 5° and plotted it with a gray line in Figure 3. The average altitude represents the particle's drift motion around the Earth. Evidently, the longitude corresponding to the minimum altitude $\overline{H}_{min}$ of the proton shows a westward shift in 2020 compared with that for the year 1900 for both L-shells. The westward shift apparent in $\overline{H}_{min}$ is caused by the westward movement of the SAA region over the past few decades. This westward movement of the SAA region has been discussed by earlier studiesPavon-Carrasco and De Santis (2016); Ye et al. (2017). Furthermore, protons initially placed at either L-shell (i.e., L =2 or 3) reached much lower altitudes in 2020 compared with the minimum altitude reached in 1900, reflecting the deeper penetration of the inner radiation belts energetic particles into the Earths atmosphere in the SAA region in 2020.

$\overline{H}$ represents the quantified average penetration altitude of the trapped 10 MeV proton in the equatorial plane. We performed different simulation runs to examine the variation of $\overline{H}$ by considering the magnetic field variation from 1900 to 2020 at 10-year intervals and estimated the value of $\overline{H}_{min}$. Simultaneously, we noted the minimum magnetic field intensity B_{min} for those years for a given L-shell. Figure 4(a) and (c) shows the variation of B_{min} with time at L =2 (red) and L =3 (blue), respectively. Notably the magnetic field intensity decreases as we move away from the Earth. Figure 4(b) and (d) shows the time variation of $\overline{H}_{min}$ for L = 2 (red) and L = 3 (blue) is shown, re-

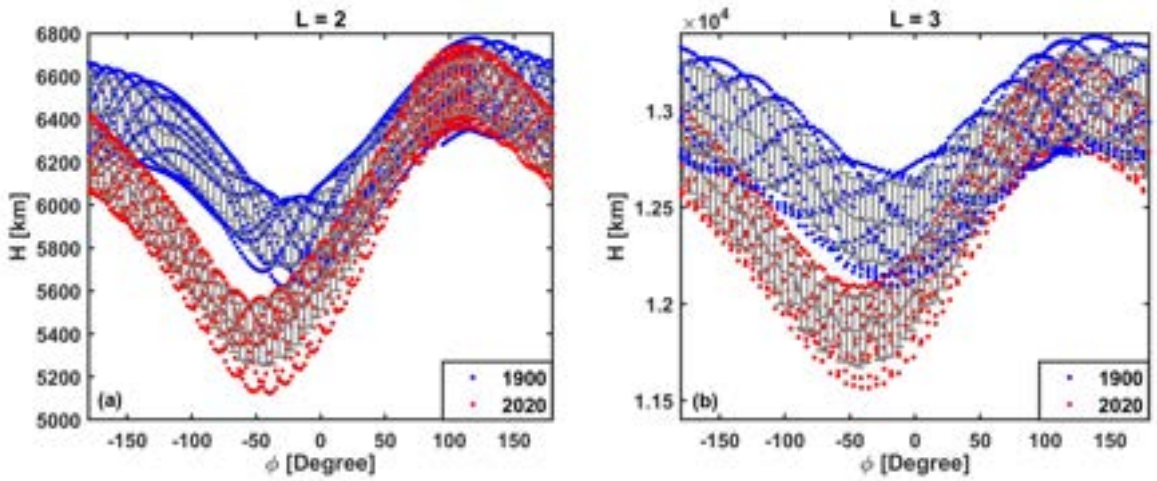

Figure 3. Variation of the 10 MeV protons altitude $H = r - R_e$ from the Earths surface as a function of the geographic longitude for the years 2020 (red) and 1900 (blue) for different initial locations of the proton: (a) L =2 and (b) L =3. These L-shell values correspond to initial altitudes of H_0=1R_e and 2R_e above the Earths surface in the equatorial plane, respectively. The gray lines represent the average altitude $\overline{H}$ of the bouncing proton with errorbar for a given fixed geographic longitudes.

spectively. Clearly, both $B_{\rm min}$, and $\overline{H}_{\rm min}$ are decreasing linearly with time from 1900 to 2020. Figure 4(b)(d) shows that this steady and consistent decrease in the magnetic field over the past few decades had direct implications for the energetic particles drifting around the Earth. We applied a least-squares fit to the variations in Figure 4, and their regression equations are given in the respective subplots. These equations indicate that the minimum altitude reached by the energetic proton in the SAA region has been decreasing at the rate of 4.1±0.1 km/year.

We computed the depth (δ) of proton in SAA region by considering its deviation from the initial position i.e., $\delta = H_0 - \overline{H}_{min}$. We obtained the empirical relation between δ and B_{min} to understand the effect of decreasing magnetic field on the lowest possible depth of the radiation belt particles. Figure 5(a) and (b) shows the δ as a function of B_{min} for L =2 (red) and L =3 (blue) for the years 1900 to 2020. The vertical black arrows indicate the years 1900 and 2020. These linear variation is fitted with the least square method for respective L-shells and the fitted lines are shown by dashed lines. The corresponding least square fit equations are given in respective subplots in Figure 5. Clearly, the variation of δ with B_{min} has different slopes for the different L-shells. This is because the magnetic field intensity varies with the altitude. It is clearly evident that proton has reached higher depths in 2020 as compare to 1900 for both L = 2 and 3. It is found that the δ has increased almost by Δ =447-543 km in year 2020 as compare to 1900 for L =2-3. This implies that in the year 2020 the inner radiation belt protons with given energy and initiated at a given L-shell are penetrating 447-543 km more deeper compared with their penetration level in 1900.

Here, we have presented simulation results for a 10 MeV proton initially placed at two different L-shells in the inner radiation belts. We have repeated the simulation runs for protons with energies 100keV, 500keV, 1 MeV, 50 MeV, and 100 MeV to understand the effect of the proton energy on the deepening of the inner radiation belt boundary from 1900 to 2020. The estimated change in the minimum penetration altitude of the proton initially placed at L =2 during 1900-2020 is presented in Table 1. Protons with different energies were observed to approach closer to the Earth by ≈389-540 km during this

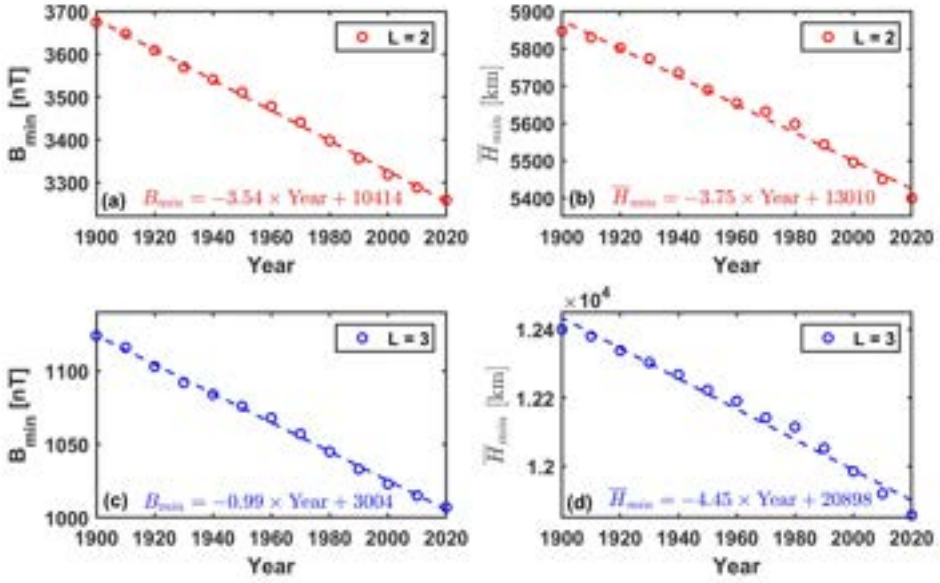

Figure 4. (a)-(c) Time variation of the minimum magnetic field intensity over the globe with time at L =2 (red), and L =3 (blue), and (b)-(d) the time variation of the minimum average penetration altitude of 10 MeV proton at L =2 (red), and L =3 (blue) for 1900-2020 in the SAA region.

period, and it was found that their penetration level was mainly controlled by magnetic field gradients ∇B in the SAA region rather than the proton energy.

Energy	L = 2			L = 3		
	δ_{1900} [km]	δ_{2020} [km]	$\Delta = \delta_{2020} - \delta_{1900}$ [km]	δ_{1900} [km]	$\delta_{2020}[km]$	$\Delta = \delta_{2020} - \delta_{1900}$
100 keV	525.1	976.3	451.2	338.0	878.2	540.2
500 keV	525.2	997.3	472.1	343.2	878.0	534.8
1 MeV	526.5	978.8	452.3	338.8	881.5	542.7
10 MeV	524.0	971.5	447.5	342.1	884.9	542.8
50 MeV	435.8	828.0	392.2	420.8	903.8	483.0
100 MeV	604.5	993.1	388.6	351.5	843.2	491.7

Table 1. The depth, $\delta = H_0 - \overline{H}_{min}$ of protons of different energy in the SAA region during 1900 and 2020. The δ in the maximum deviation of proton from its initial position.

4 Discussion and Conclusions

High radiation doses in the SAA region is a matter of great concern as they reflect the penetration of energetic particles and cosmic rays to lower altitudes. Therefore, the steady and continuous decrease in the geomagnetic field in the SAA region has direct implications for life in the region, satellites and climate. Studies have suggested that the cosmic ray flux can cause long-term changes in the Earth's climate (S. Campuzano, De Santis, Pavón-Carrasco, Osete, & Qamili, 2018; Lanci, Galeotti, Grimani, & Huber, 2020). Furthermore, it has been predicted that the steady decrease in the Earth's magnetic field

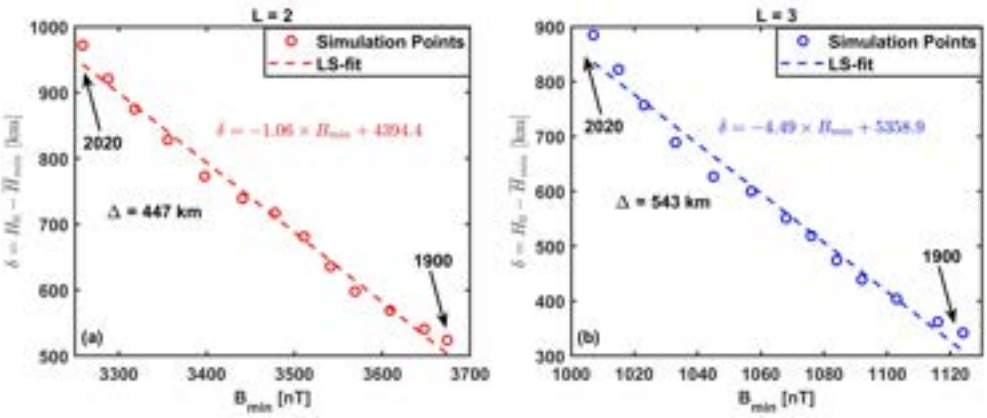

Figure 5. The variation of depth δ of 10 MeV proton initially placed at L =2 (red) and L =3 (blue) as a function of minimum geomagnetic field B_{min} at respective L-shells. Here, $\delta = H_0 - \overline{H}_{min}$. The least square (LS) fitted lines are shown by dashed lines and respective least square fit equations are mentioned in the plot.

will continue in the near future and that the magnetic moment of the Earth will decrease further (Finlay, Aubert, & Gillet, 2016). Ground and satellite observations show that the rate of decrease in the magnetic field in the SAA region has increased in the last fifty years and that there is a possibility of the anomaly splitting into two regions. It has also been recently suggested that the Earth's magnetic field can change 10 times faster than previously thought (Davies & Constable, 2020). These observations underscore the potential seriousness of the increasing penetration levels of energetic particles in the SAA region.

Since particle dynamics in the SAA region is influenced by the solar flux level and geomagnetic activity (Qin et al., 2014), long-term satellite observations of particle fluxes in the region with good altitudinal coverage are required to investigate the low-altitude penetration of high-energy particles. The limited availability of satellite observations renders the isolation of the effect of the Earth's weakening magnetic field on the low-altitude penetration challenging. In such a scenario, test-particle simulations can help to understand the effect of the decreasing magnetic field in the SAA region on the inner boundary of the radiation belt and to estimate the penetration altitude of charged particles in the region.

From the results of the present study, it is evident that the decrease in the geomagnetic field in the SAA region is causing energetic radiation belt particles to steadily approach closer to the Earth. In the last 120 years (1900-2020), the lower boundary of the radiation belt has moved approximately 480 kms toward the Earth. In such a scenario, the empirical relations presented in Figure 5 are extremely useful to understand the penetration and forecast the penetration altitude of the radiation belt particles with the knowledge of the minimum magnetic field in the SAA region. Furthermore, the simulation results can be useful in modelling the radiation level in the SAA region at future instants.

Acknowledgments

We thank NGDC NOAA for the IGRF model. The data required for simulation model is obtained from the latest 13th generation International Geomagnetic Reference Field model and available from `https://www.ngdc.noaa.gov/IAGA/vmod/igrf.html`.

References

Alken, P., Thebault, E., Beggan, C., Aubert, J., Baerenzung, J., Brown, W. J., ... others (09 Sep, 2020). Evaluation of candidate models for the 13th generation international geomagnetic reference field. *Version-2 available at Research Square*. doi: 10.21203/rs.3.rs-41022/v2

Campuzano, S., De Santis, A., Pavón-Carrasco, F. J., Osete, M. L., & Qamili, E. (2018). New perspectives in the study of the earths magnetic field and climate connection: The use of transfer entropy. *PloS one*, *13*(11), e0207270. doi: 10.1371/journal.pone.0207270

Campuzano, S. A., Gómez-Paccard, M., Pavón-Carrasco, F. J., & Osete, M. L. (2019). Emergence and evolution of the south atlantic anomaly revealed by the new paleomagnetic reconstruction shawq2k. *Earth and Planetary Science Letters*, *512*, 17–26. doi: 10.1016/j.epsl.2019.01.050

Chen, F. F., et al. (1984). *Introduction to plasma physics and controlled fusion* (Vol. 1). Springer.

Chen, M. W., Roeder, J. L., Fennell, J. F., Lyons, L. R., Lambour, R. L., & Schulz, M. (1999). Proton ring current pitch angle distributions: Comparison of simulations with crres observations. *Journal of Geophysical Research: Space Physics*, *104*(A8), 17379–17389. doi: 10.1029/1999JA900142Citations

Davies, C. J., & Constable, C. G. (2020). Rapid geomagnetic changes inferred from earth observations and numerical simulations. *Nature communications*, *11*(1), 1–10. doi: 10.1038/s41467-020-16888-0

Ebihara, Y., & Miyoshi, Y. (2011). Dynamic inner magnetosphere: A tutorial and recent advances. In *The dynamic magnetosphere* (pp. 145–187). Springer. doi: 10.1007/978-94-007-0501-2

Finlay, C. C., Aubert, J., & Gillet, N. (2016). Gyre-driven decay of the earths magnetic dipole. *Nature communications*, *7*(1), 1–8. doi: 10.1038/ncomms10422

Finlay, C. C., Olsen, N., Kotsiaros, S., Gillet, N., & Tøffner-Clausen, L. (2016). Recent geomagnetic secular variation from swarm and ground observatories as estimated in the chaos-6 geomagnetic field model. *Earth, Planets and Space*, *68*(1), 112. doi: 10.1186/s40623-016-0486-1

Gillet, N., Jault, D., Finlay, C., & Olsen, N. (2013). Stochastic modeling of the earth's magnetic field: Inversion for covariances over the observatory era. *Geochemistry, Geophysics, Geosystems*, *14*(4), 766–786. doi: 10.1002/ggge.20041

Heirtzler, J. R. (2002). The future of the south atlantic anomaly and implications for radiation damage in space. *Journal of Atmospheric and Solar-Terrestrial Physics*, *64*(16), 1701–1708. doi: 10.1016/S1364-6826(02)00120-7

Lanci, L., Galeotti, S., Grimani, C., & Huber, M. (2020). Evidence against a long-term control on earth climate by galactic cosmic ray flux. *Global and Planetary Change*, *185*, 103095. doi: 10.1016/j.gloplacha.2019.103095

Liu, L., & Olson, P. (2009). Geomagnetic dipole moment collapse by convective mixing in the core. *Geophysical research letters*, *36*(10). doi: 10.1029/2009GL038130

Millan, R., & Baker, D. (2012). Acceleration of particles to high energies in earths radiation belts. *Space Science Reviews*, *173*(1-4), 103–131. doi: 10.1007/s11214-012-9941

Mukherjee, G., & Rajaram, R. (1981). Motion of charged particles in the magnetosphere. *Astrophysics and Space Science*, *74*(2), 287–301. doi: 10.1007/BF00656440

Navabi, M., & Barati, M. (2017). Mathematical modeling and simulation of the earth's magnetic field: A comparative study of the models on the spacecraft attitude control application. *Applied Mathematical Modelling*, *46*, 365–381. doi: 10.1016/j.apm.2017.01.040

Northrop, T. G., & Teller, E. (1960). Stability of the adiabatic motion of charged particles in the earth's field. *Physical Review*, *117*(1), 215. doi: 10.1103/

PhysRev.117.215
Öztürk, M. K. (2012). Trajectories of charged particles trapped in earths magnetic field. *American Journal of Physics*, *80*. doi: 10.1119/1.3684537
Pavon-Carrasco, F. J., & De Santis, A. (2016). The south atlantic anomaly: The key for a possible geomagnetic reversal. *Frontiers in Earth Science*, *4*, 40. doi: 10.3389/feart.2016.00040
Qin, M., Zhang, X., Ni, B., Song, H., Zou, H., & Sun, Y. (2014). Solar cycle variations of trapped proton flux in the inner radiation belt. *Journal of Geophysical Research: Space Physics*, *119*(12), 9658–9669. doi: 10.1002/2014JA020300
Ripoll, J.-F., Claudepierre, S. G., Ukhorskiy, A. Y., Colpitts, C., Li, X., Fennell, J. F., & Crabtree, C. (2020). Particle dynamics in the earth's radiation belts: Review of current research and open questions. *Journal of Geophysical Research: Space Physics*, *125*(5), e2019JA026735. doi: 10.1029/2019JA026735
Rodrigues, R. R., Taschetto, A. S., Gupta, A. S., & Foltz, G. R. (2019). Common cause for severe droughts in south america and marine heatwaves in the south atlantic. *Nature Geoscience*, *12*(8), 620–626. doi: 10.1038/s41561-019-0393-8
Soni, P. K., Kakad, B., & Kakad, A. (2020a). L-shell and energy dependence of magnetic mirror point of charged particles trapped in earths magnetosphere. *Earth, Planets and Space*, *72*(1), 1–15. doi: 10.1186/s40623-020-01264-5
Soni, P. K., Kakad, B., & Kakad, A. (2020b). Simulation study of motion of charged particles trapped in earths magnetosphere. *Advances in Space Research*. doi: 10.1016/j.asr.2020.10.020
Suttie, N., Holme, R., Hill, M. J., & Shaw, J. (2011). Consistent treatment of errors in archaeointensity implies rapid decay of the dipole prior to 1840. *Earth and Planetary Science Letters*, *304*(1-2), 13–21. doi: 10.1016/j.epsl.2011.02.010
Thébault, E., Finlay, C. C., Beggan, C. D., Alken, P., Aubert, J., Barrois, O., ... others (2015). International geomagnetic reference field: the 12th generation. *Earth, Planets and Space*, *67*(1), 79. doi: 10.1186/s40623-015-0228-9
Ye, Y., Zou, H., Zong, Q., Chen, H., Wang, Y., Yu, X., & Shi, W. (2017). The secular variation of the center of geomagnetic south atlantic anomaly and its effect on the distribution of inner radiation belt particles. *Space Weather*, *15*(11), 1548–1558. doi: doi.org/10.1002/2017SW001687
Zhu, C., & Liu, Z. (2020). Weakening atlantic overturning circulation causes south atlantic salinity pile-up. *Nature Climate Change*, 1–6. doi: 10.1038/s41558-020-0897-7